SOME APPLICATIONS OF THE NASTRAN LEVEL 16 SUBSONIC FLUTTER ANALYSIS CAPABILITY

Robert V. Doggett, Jr., and Herbert J. Cunningham
NASA Langley Research Center

ABSTRACT AND SUMMARY

Results are presented that were obtained by applying the new Level 16 flutter analysis capability to an aspect-ratio-6.8 subsonic-transport-type wing, an aspect-ratio-1.7 arrow wing, and an aspect-ratio-1.3 all-movable horizontal tail with a geared elevator. The transport wing and arrow-wing results are compared with experimental results obtained in the Langley transonic dynamic tunnel and with other calculated results obtained using subsonic lifting surface (kernel function) unsteady aerodynamic theory.

INTRODUCTION

Improvements in the NASA structural analysis computer program (NASTRAN) have been made continuously since the first public release of the program in 1970. These improvements have included both the upgrading of capability that was included in the initial public version and the addition of new analysis capabilities that were not included previously. One new capability that is generally available in a standard level for the first time with the release of Level 16 is subsonic flutter analysis. The flutter analysis is organized into a new rigid format, APP AERO, SOL 10. The features and capabilities of the Level 16 flutter analysis are the same as those of the analysis originally installed in a nonstandard Level 15.1 version (see refs. 1 and 2). As presently implemented, the analysis is applicable to multiple, nonplanar, mutually interfering lifting surfaces. The analysis is of the modal type. That is, the flutter equations are formulated in terms of generalized modal coordinates using a finite number of the natural modes of the structure. These modes and frequencies are determined using a conventional NASTRAN finite-element structural model. The solution of the flutter equations is accomplished by the traditional k-method. The generalized unsteady aerodynamic forces are determined using doublet lattice unsteady aerodynamic theory which requires that the lifting surface be divided into an array of trapezoidal boxes. As implemented in NASTRAN, there is an aerodynamic grid point located at the center of each of these boxes. The interconnection of the aerodynamic and structural models is accomplished by using one-dimensional and surface spline functions to interpolate the modal displacements determined at the structural grid points to displacements and slopes required at the aerodynamic grid points. The generality of this structural-aerodynamic interface allows the user to select a structural model that is best suited from structural considerations alone and an aerodynamic model that is dictated by aerodynamic considerations alone. Capability is provided for interpolating the generalized aerodynamic forces determined at

specific values of the independent aerodynamic parameter, Mach number, or reduced frequency, to forces at intermediate values of these parameters.

The purpose of this paper is to present NASTRAN flutter results for three different configurations; namely, an aspect-ratio-6.8 subsonic-transport-type wing, an aspect-ratio-1.7 arrow wing, and an aspect-ratio-1.3 all-movable horizontal tail with a geared-elevator control surface. The NASTRAN flutter results for the transport wing and arrow wing are compared with wind-tunnel model experimental results obtained in the Langley transonic dynamics tunnel and with other calculated results obtained by using subsonic lifting surface (kernel function) unsteady aerodynamic theory. The kernel function results were obtained using NASTRAN calculated modes and frequencies and flutter analysis methods similar to those contained in NASTRAN, such as surface spline interpolation, generalized aerodynamic force interpolation, and the k-method of solution. All NASTRAN flutter results presented were obtained using standard Level 16 as installed on the CDC 6000 series computers at the Langley Research Center.

APPLICATIONS

Subsonic Transport Wing

The subsonic-transport wing for which NASTRAN flutter results were obtained was one of two wind-tunnel models tested in the Langley transonic dynamics tunnel to study possible supercritical-airfoil-section effects on flutter (see ref. 3). A photograph of the swept, tapered, aspect-ratio-6.8 cantilever-mounted wing installed on a fuselage half-body in the wind tunnel is presented in figure 1. The wing geometry, the structural model, and one of the aerodynamic models used (doublet lattice box arrangement) are presented in figure 2. Although the model construction was rather complex (fiberglass skins stabilized by a full-depth honeycomb core with ballasting weights inserted in the core), the wing was essentially a beamlike structure so NASTRAN BAR elements were used in the structural model. The aerodynamic model shown in figure 2 contains 100 doublet lattice boxes, five boxes along the chord at each of 20 span stations. The aerodynamic model in the figure was the basic one used in the flutter analysis, but additional calculations were made using 50 boxes, five per chord at 10 span stations, and also 200 boxes, five per chord at 40 span stations. Note that the aerodynamic planform is slightly different from the actual planform near the wing root and tip since curved planform edges are approximated by the straight line segments of the doublet lattice boxes.

The first six calculated natural modes and frequencies of the wing were used in the flutter analysis. Oblique projections of the calculated mode shapes and the corresponding natural frequencies are shown in figure 3. Also included in the figure are the measured natural frequencies. The measured and calculated natural frequencies are in good agreement and, although not shown in this figure, the calculated mode shapes are very similar to the measured mode shapes. One-dimensional spline functions were used to interpolate the modal displacements in the flutter analysis.

The flutter results are presented in figure 4 as the variations of the flutter frequency and dynamic pressure with Mach number. The NASTRAN results are indicated by the symbols in this figure. Also included are the experimental flutter results (from ref. 3) and calculated results obtained using subsonic lifting surface (kernel function) theory (ref. 4). A six-by-six collocation point arrangement was used for the kernel function calculations. Both sets of calculated results predict higher flutter frequencies and dynamic pressures than were found experimentally. Although the kernel function results are in better agreement with the experiment than the NASTRAN results, the differences between the two calculations are not considered to be large and are not untypical of differences that occur in flutter analyses using different unsteady aerodynamic theories. The NASTRAN results at Mach number 0.934 using 50, 100, and 200 doublet lattice boxes show that the 100-box and 200-box results are virtually the same, and that the 50-box results are only slightly higher.

Arrow Wing

The arrow-wing configuration was another wind-tunnel model and is shown mounted in the wind tunnel in figure 5. The aspect-ratio-1.7, cantilever-mounted model is a simplified 0.02-size version of the Supersonic Cruise Aircraft Research (SCAR) arrow-wing design. The experimental flutter data obtained for this model will be used in validating flutter analysis methods applicable to the arrow-wing configuration. The model geometry, structural model, and aerodynamic model are presented in figure 6. The arrow-wing model was of simple construction, being an aluminum-alloy plate covered with balsa wood to give the desired airfoil shape. The structural model consisted of NASTRAN QUAD2 and TRIA2 plate-bending elements. The basic aerodynamic model shown in figure 6 consisted of 108 doublet lattice boxes, nine along the chord at each of 12 span stations. Some calculations were made using 60 boxes, 5 by 12, and 189 boxes, 9 by 21. Note that the aerodynamic model planform is slightly different from the geometric planform.

The first five calculated natural modes were used in the flutter analysis. Oblique projections of the calculated mode shapes along with the corresponding natural frequencies are presented in figure 7. Also included in the figure are the measured natural frequencies. The calculated and measured frequencies are in reasonably good agreement. Surface-spline functions were used to interpolate the modal displacements at the structural grid points to displacements and slopes required for each doublet lattice box.

The flutter results are presented in figure 8 as the variations of the flutter frequency and dynamic pressure with Mach number. Also included in the figure are calculated results obtained using kernel function unsteady aerodynamic theory (ref. 4) and some previously unpublished experimental flutter results obtained in the Langley transonic dynamics tunnel by the first author and Rodney H. Ricketts of the Vought Corporation, Hampton Technical Center. A six-by-six collocation point arrangement was used in the kernel function analysis. The NASTRAN results are in good agreement with the experiment. The kernel function results indicate a flutter boundary lower than NASTRAN and the experimental results. The NASTRAN results at 0.9 Mach number using 60, 108,

and 189 doublet lattice boxes show that the 108-box and 189-box results are virtually the same, and that the 60-box results are slightly higher.

All-Movable Horizontal Tail

The third configuration which was studied is the aspect-ratio-1.3 all-movable horizontal tail with geared elevator shown in the upper left sketch in figure 9. This configuration is being used in a study to provide a better understanding of the effects of elevator-gear ratio on flutter. Some initial results from this study are presented here. Elevator gear ratio as used herein is defined by the sketch shown at the lower left in figure 9. Also included in figure 9 is the basic aerodynamic model used. This model is a purely analytical representation, that is, no physical model exists for which experimental flutter data have been obtained.

The configuration consists of a stabilizer portion which can translate and rotate about the stabilizer pitch axis which is located at 40 percent of the root chord. A full-span elevator with unswept hinge line is hinged to the stabilizer. The elevator hinge line is at 75 percent of the root chord. Since the stabilizer and elevator were analyzed as rigid surfaces, there are no camber or bending deformations. The horizontal tail was modeled structurally using spring (CELAS2) elements to represent the translational, pitch, and elevator-rotational stiffnesses. The mass and inertia of the stabilizer and elevator were modeled using concentrated masses (CONM2). The elevator gearing was effected by using multipoint constraints (MPC's). Oblique projections of the calculated mode shapes for the 2 to 1 gear-ratio configuration are shown in figure 10. It should be pointed out that since the elevator rotational stiffness spring was in series with the gearing mechanism, the elevator rotational angles in the mode shapes are not simply the stabilizer pitch angle times the gear ratio. The calculated natural frequencies for all gear ratios studied are tabulated on this figure. Note that the mode shapes are composed of varying combinations of vertical translation, stabilizer pitch, and elevator rotation. The mode shapes for the other gear ratios studied are similar to those shown in the figure, the primary differences being in relative angular rotation between the stabilizer and elevator. Also note that increasing the elevator gear ratio had little effect on the first-mode frequency while the second-mode frequency systematically decreased and the third-mode frequency systematically increased as the gear ratio was increased.

To meet the purposes of the present study, it was not only necessary to have a simple structural model to facilitate the changing of structural parameters, but it was also desired to have a simple aerodynamic model (minimum number of doublet lattice boxes) in order to keep computational costs low since the CPU time required for the unsteady aerodynamic forces is approximately proportional to the square of the number of boxes. Since the 25-box arrangement shown in figure 9 gave results essentially the same as a large 100-box arrangement, this admittedly coarse model was used as the basic aerodynamic model. Surface spline functions were used to interpolate the modal displacements. A separate spline function was used for the stabilizer and elevator in order to account properly for the geometric discontinuity in the downwash that occurs at the elevator hinge line.

The calculated flutter results are presented in figure 11 as the variation of flutter frequency and dynamic pressure with elevator gear ratio. All calculations were made for a density of 0.515 kg/m^3 (42 percent of sea-level standard air density) at a Mach number of 0.80. Both the flutter dynamic pressure and frequency increase as the gear ratio is increased indicating that gearing the elevator is mildly favorable from a flutter point of view. The trend of these data is consistent with that presented in reference 5 where wind-tunnel flutter results are presented for a relatively complex geared-elevator model having a planform similar to the one used here.

CONCLUDING REMARKS

Results from applying the NASTRAN Level 16 subsonic flutter analysis (which uses doublet lattice unsteady aerodynamic theory) to three configurations have been presented. The three configurations studied were (1) a swept, tapered, aspect-ratio-6.8 subsonic-transport-type wing, (2) an aspect-ratio-1.7 arrow wing which is representative of supersonic cruise aircraft configurations of current interest, and (3) an aspect-ratio-1.3 all-movable horizontal tail with a geared-elevator control surface. The NASTRAN results for the subsonic-transport wing and the arrow wing were in good agreement with wind-tunnel model experimental flutter results and were consistent with other calculated flutter results obtained using subsonic lifting surface (kernel function) unsteady aerodynamic theory. The NASTRAN results for the horizontal-tail configuration with geared elevator indicated a gradual increase in flutter frequency and dynamic pressure with increasing gear ratio. Although no experimental and other calculated results are available for the specific horizontal tail studied here, the trends of the NASTRAN results are the same as those determined in reference 5 for a similar, but more complex, configuration.

REFERENCES

1. Doggett, Robert V., Jr.; and Harder, Robert L.: Subsonic Flutter Analysis Addition to NASTRAN. NASTRAN: User's Experiences. NASA TM X-2893, September 1973, pp. 507-529.

2. Jew, Howard: Delta Wing Flutter Based on Doublet Lattice Method in NASTRAN. NASTRAN: User's Experiences. NASA TM X-3278, September 1975, pp. 603-613.

3. Farmer, Moses G.; and Hanson, Perry W.: Comparison of Supercritical and Conventional Wing Flutter Characteristics. Proceedings AIAA/ASME/SAE 17th Structures, Structural Dynamics, and Materials Conference (King of Prussia, PA), May 5-7, 1976, pp. 308-614. (Also available as NASA TM X-72837.)

4. Watkins, Charles E.; Woolston, Donald S.; and Cunningham, Herbert J.: A Systematic Kernel Function Procedure for Determining Aerodynamic Forces on Oscillating or Steady Finite Wings at Subsonic Speeds. NASA TR R-48, 1959.

5. Ruhlin, Charles L.; Doggett, Robert V., Jr.; and Gregory, Richard A.: Geared-Elevator Flutter Study. Proceedings AIAA/ASME/SAE 17th Structures, Structural Dynamics, and Materials Conference (King of Prussia, PA), May 5-7, 1976, pp. 598-607.

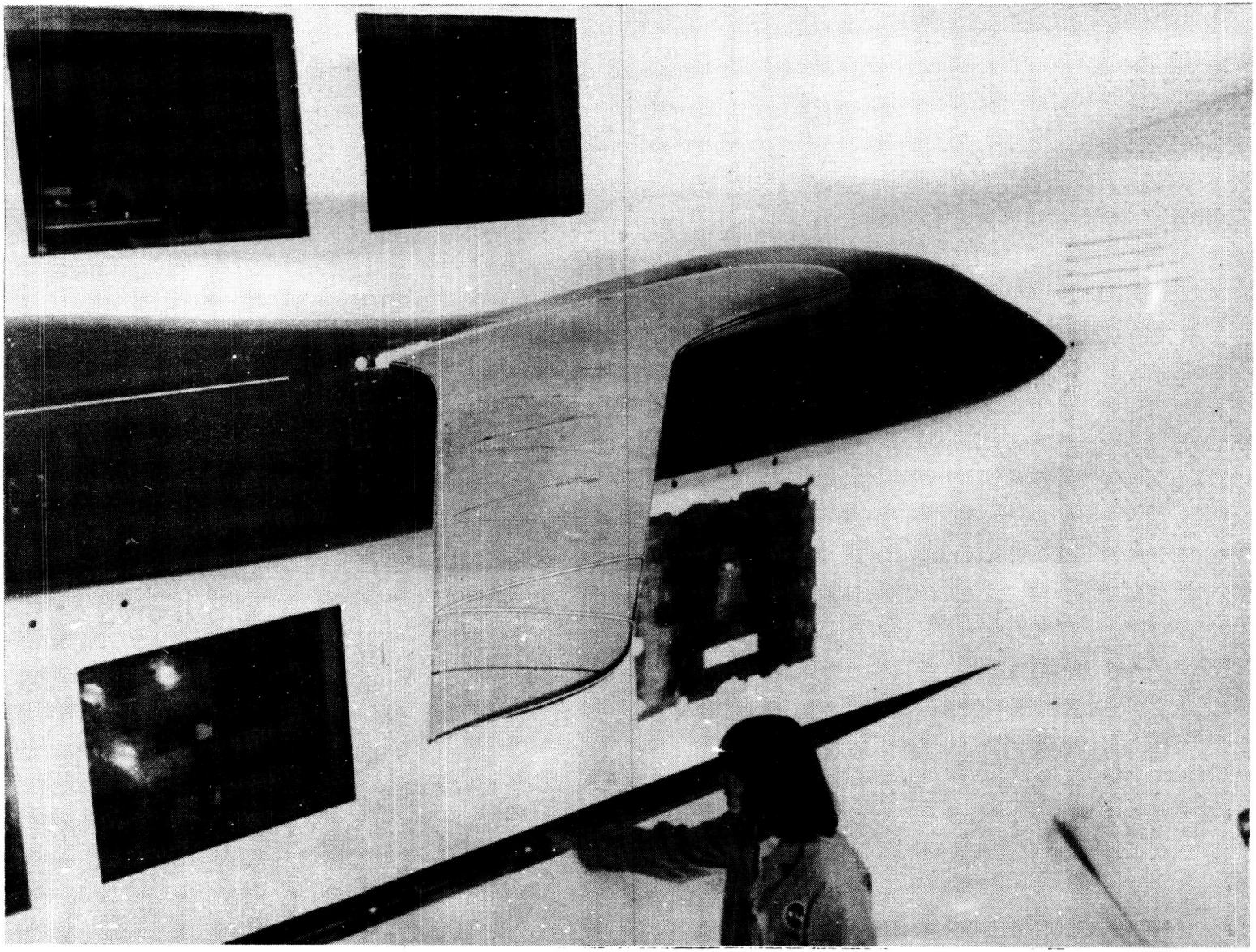

Figure 1. Subsonic-transport wing mounted in transonic dynamics tunnel.

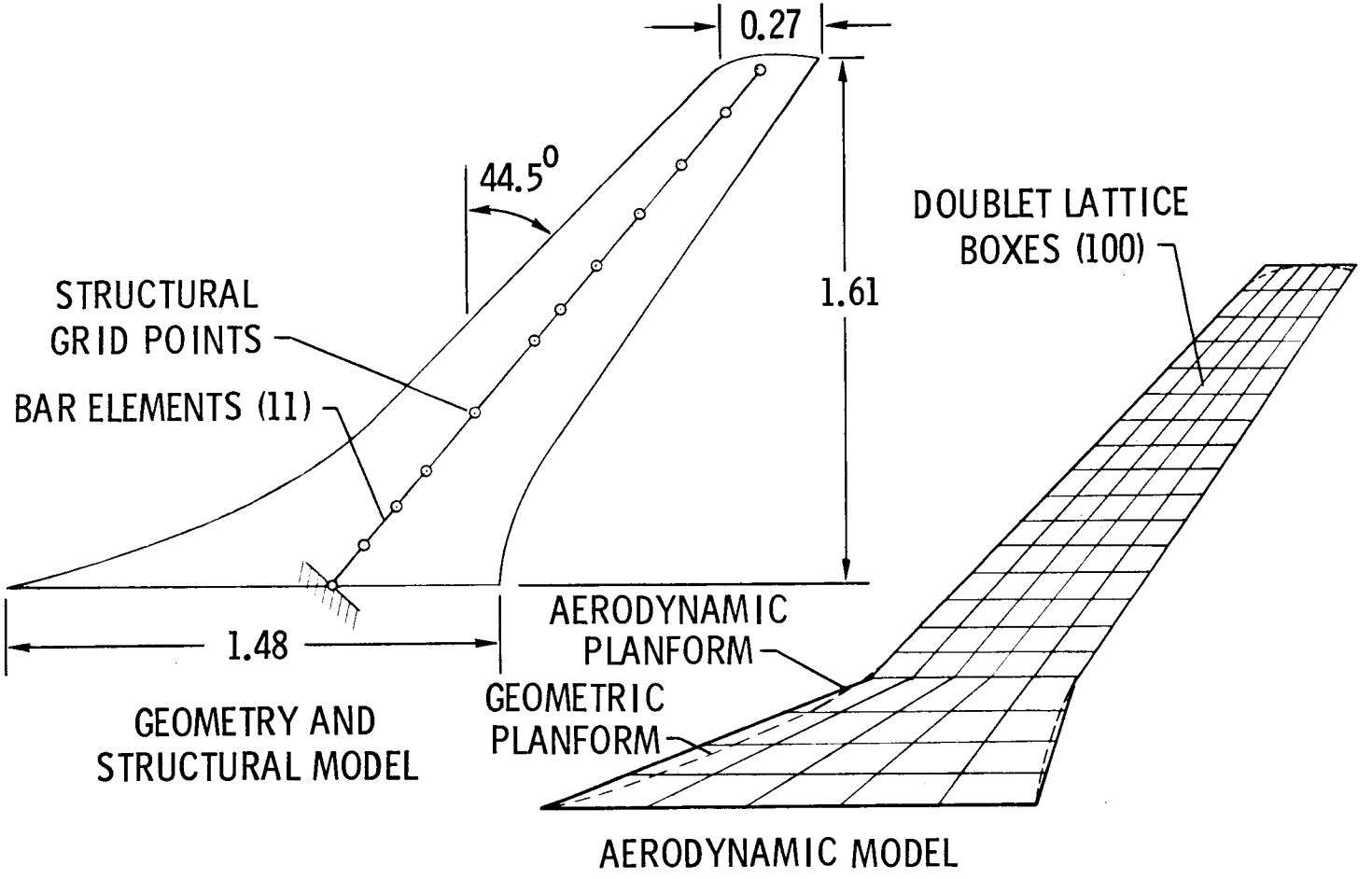

Figure 2. Subsonic-transport-wing geometry, structural model, and aerodynamic model. All dimensions are in meters.

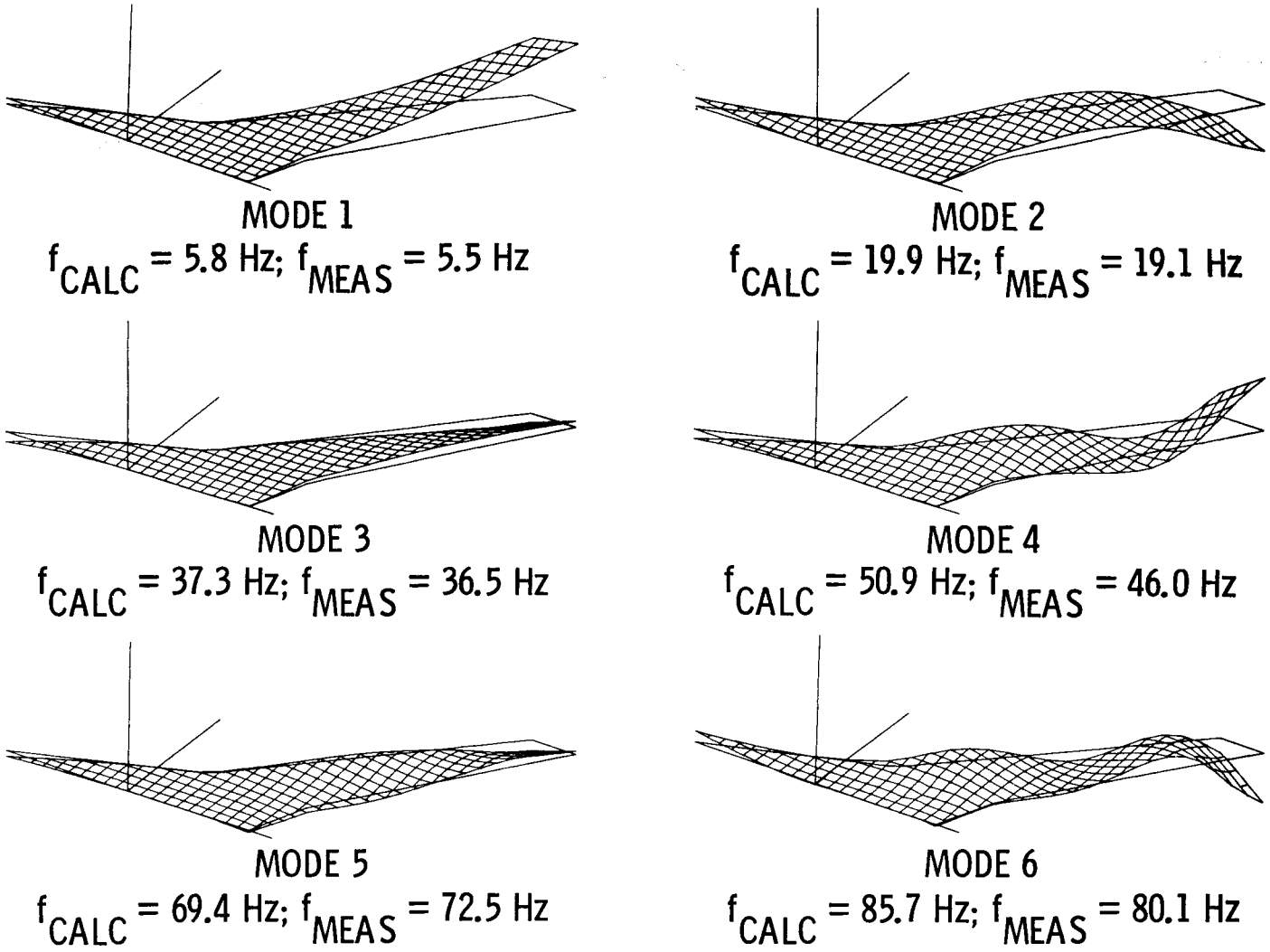

Figure 3. Subsonic-transport-wing mode shapes and frequencies.

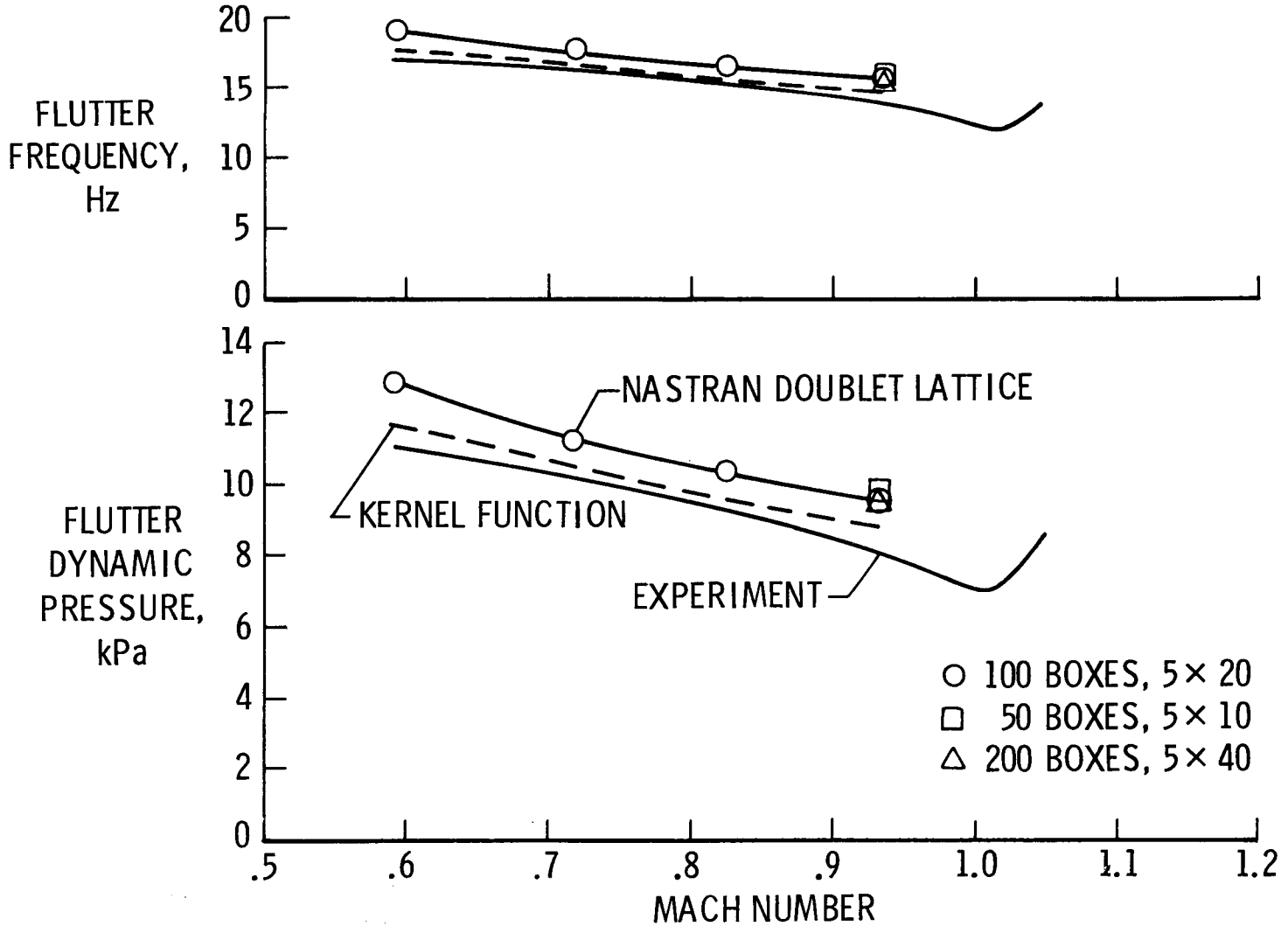

Figure 4. Subsonic-transport-wing flutter results.

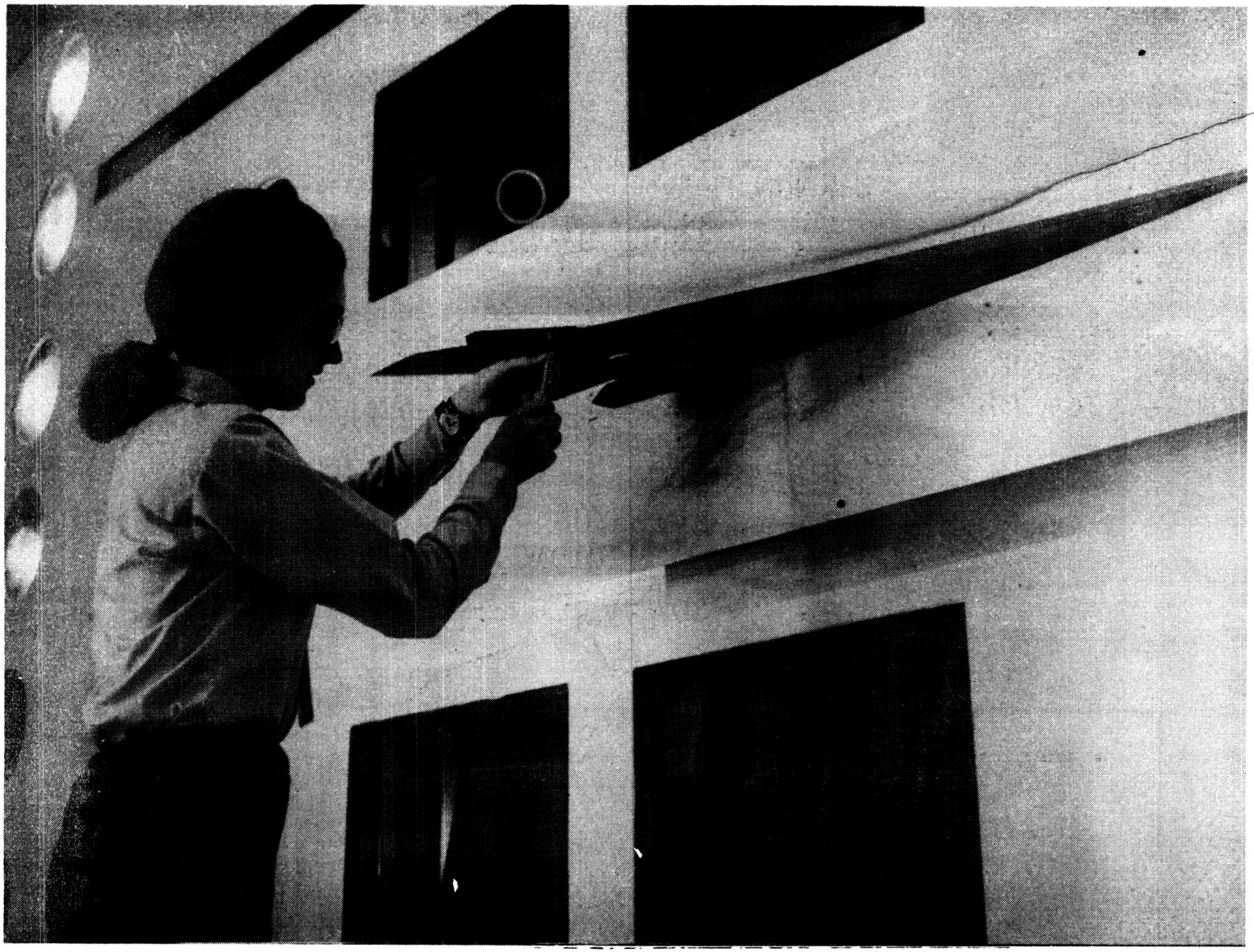

Figure 5. Arrow wing mounted in transonic dynamics tunnel.

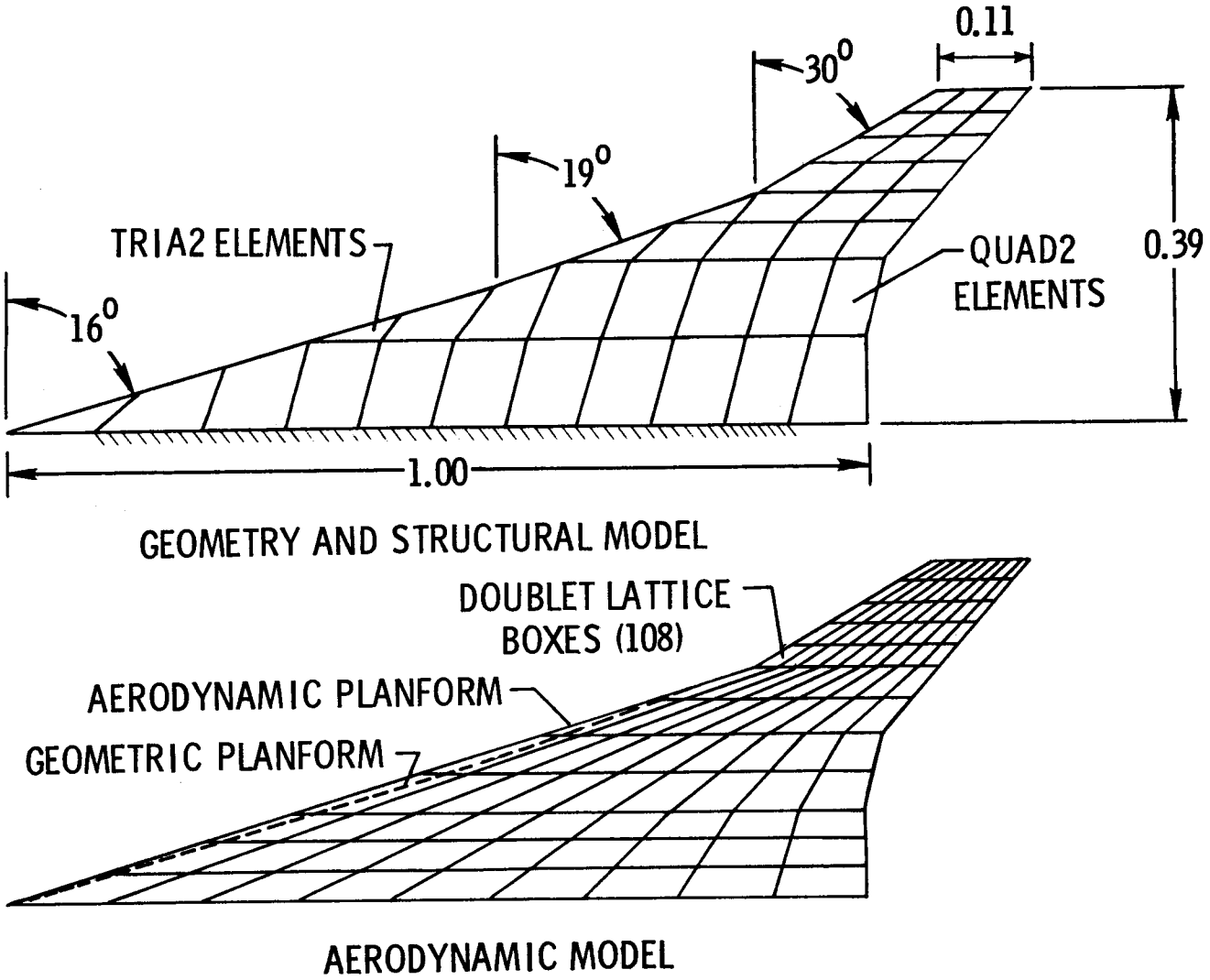

Figure 6. Arrow-wing geometry, structural model, and aerodynamic model. All dimensions are in meters.

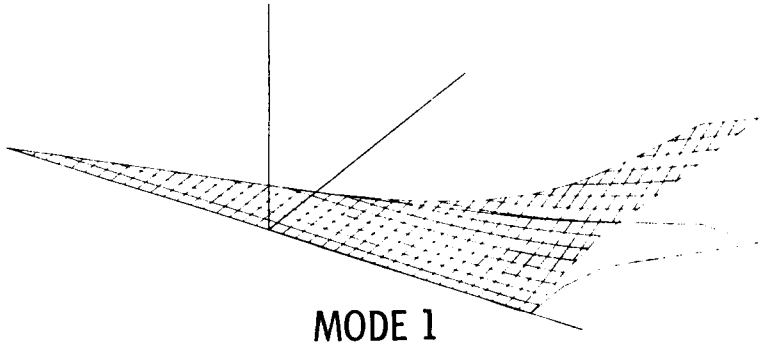

MODE 1

f_{CALC} = 13.2 Hz; f_{MEAS} = 12.9 Hz

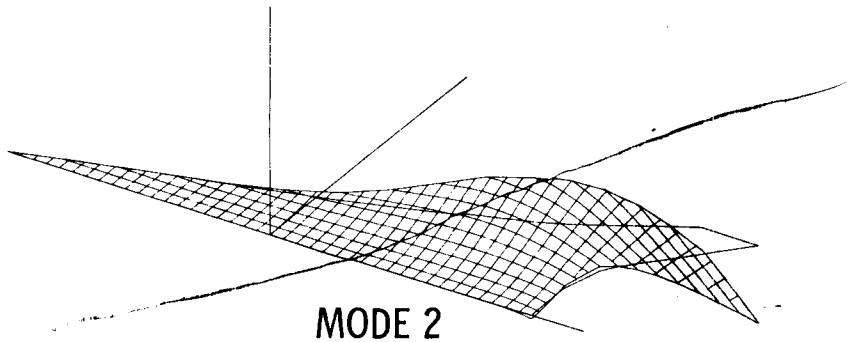

MODE 2

f_{CALC} = 43.4 Hz; f_{MEAS} = 44.1 Hz

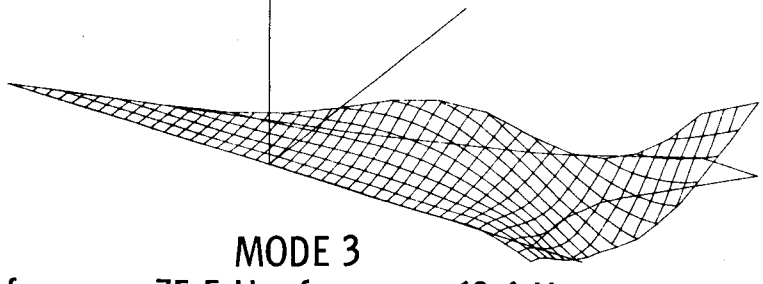

MODE 3

f_{CALC} = 75.5 Hz; f_{MEAS} = 69.6 Hz

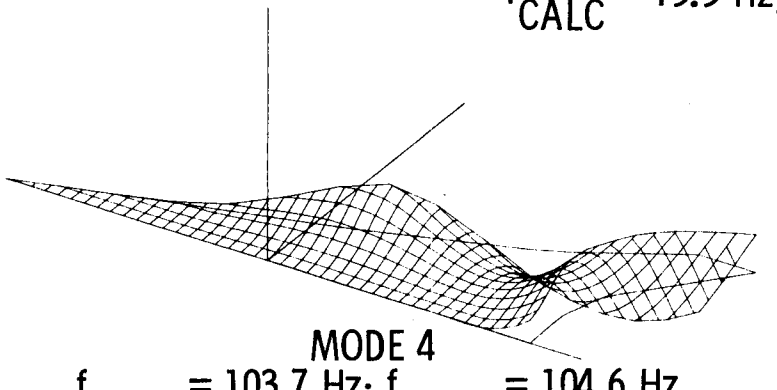

MODE 4

f_{CALC} = 103.7 Hz; f_{MEAS} = 104.6 Hz

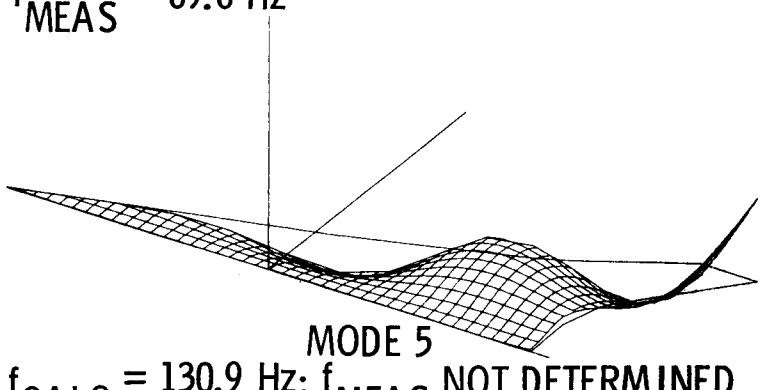

MODE 5

f_{CALC} = 130.9 Hz; f_{MEAS} NOT DETERMINED

Figure 7. Arrow-wing mode shapes and frequencies.

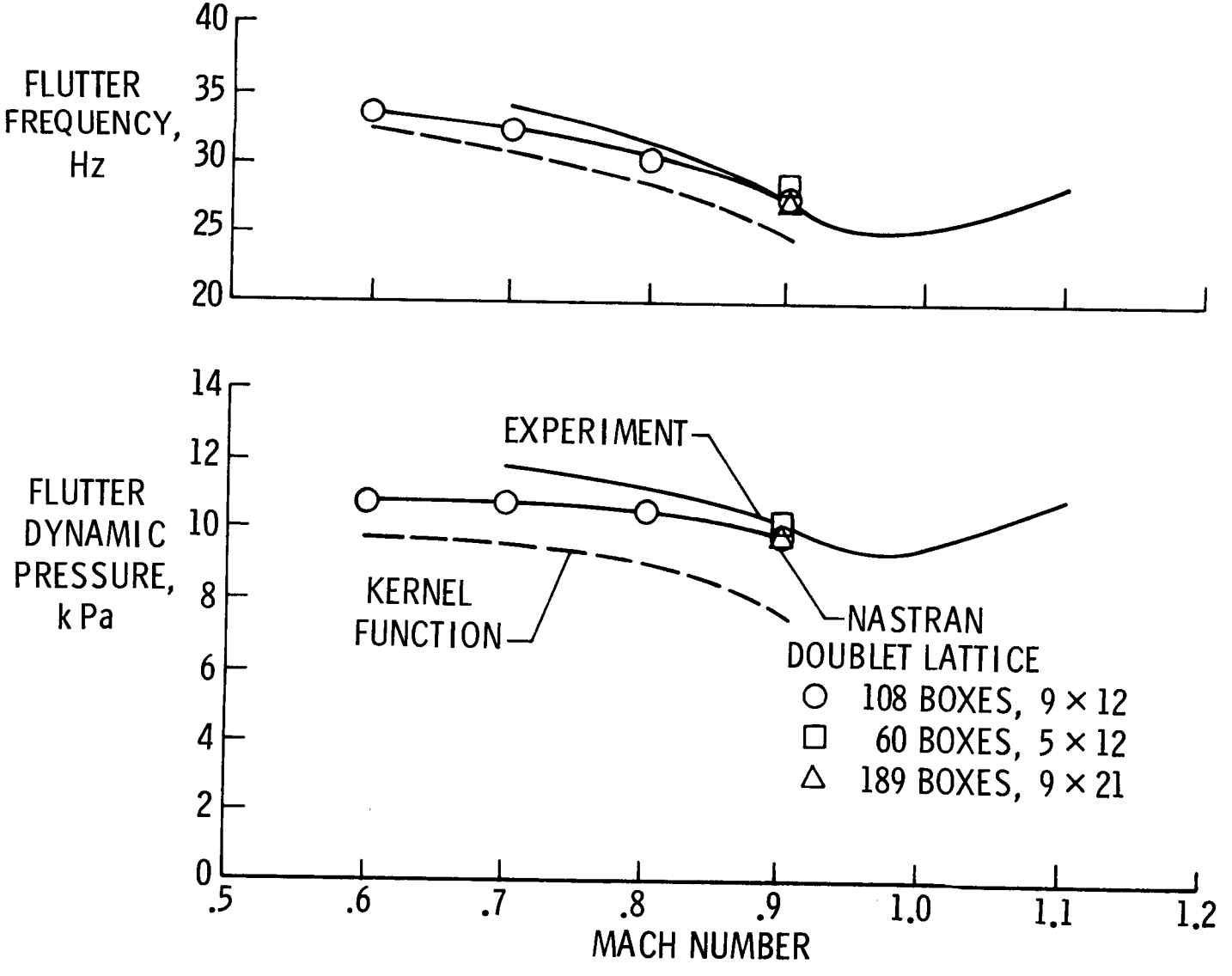

Figure 8. Arrow-wing flutter results.

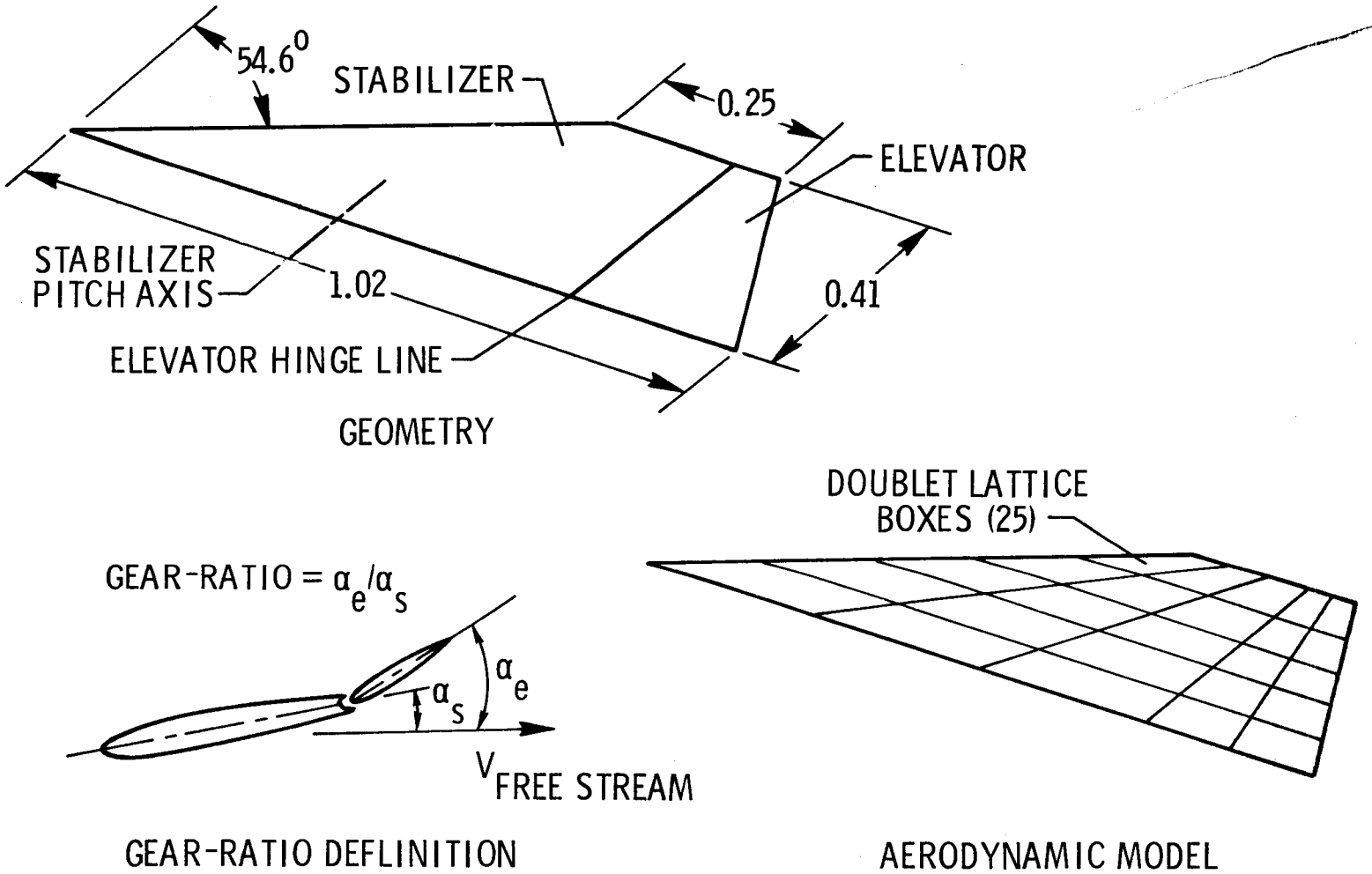

Figure 9. All-movable horizontal tail geometry, aerodynamic model, and gear-ratio definition. All dimensions are in meters.

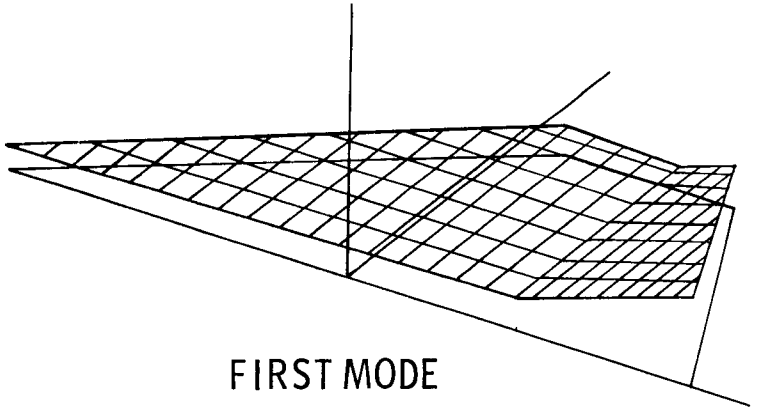

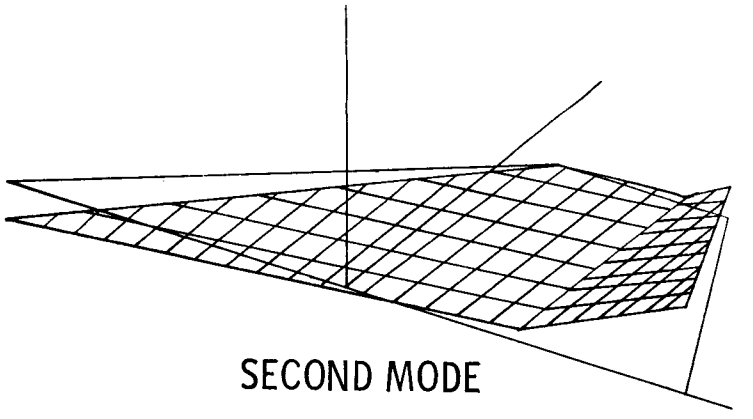

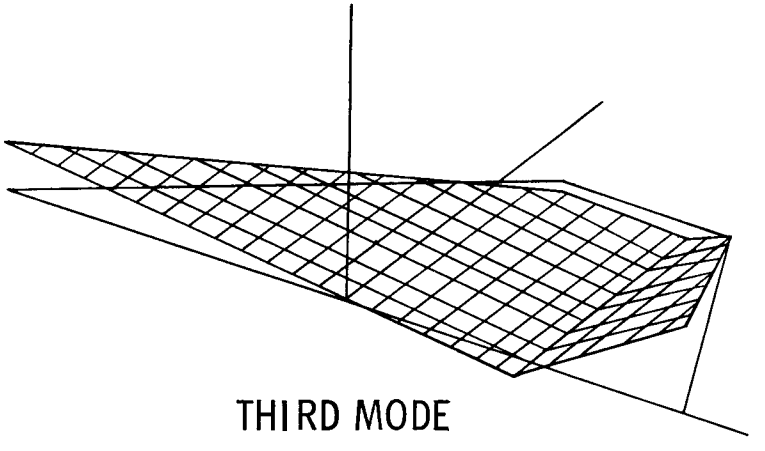

	CALCULATED NATURAL FREQUENCIES, Hz		
GEAR-RATIO	FIRST MODE	SECOND MODE	THIRD MODE
1.0 : 1	6.9	21.6	35.6
1.5 : 1	6.9	20.4	37.6
2.0 : 1	6.9	19.4	39.7
2.5 : 1	6.9	18.4	41.9
3.0 : 1	6.9	17.5	44.2

Figure 10. All-movable horizontal tail mode shapes and frequencies.

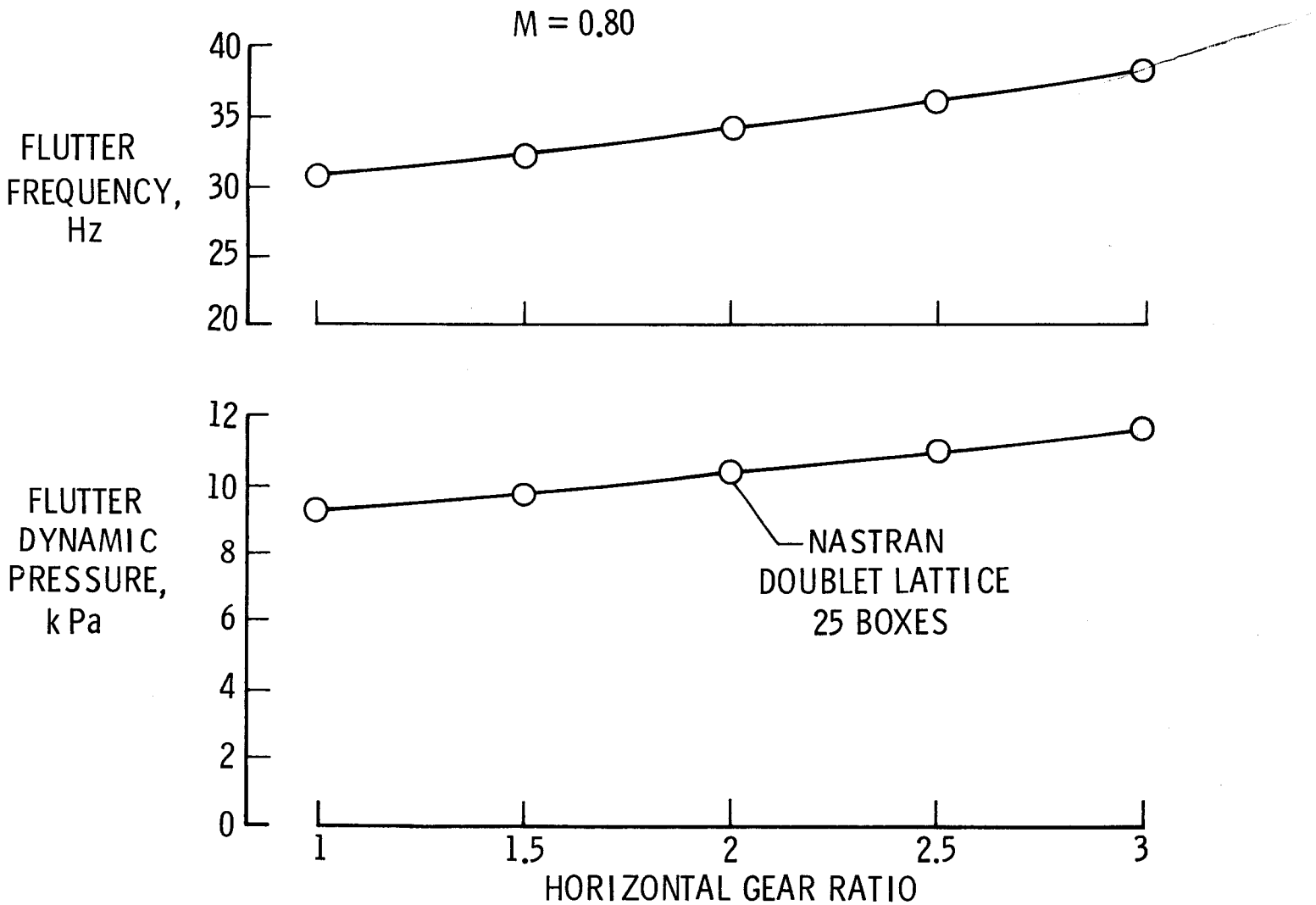

Figure 11. All-movable horizontal tail flutter results.